Structural factors determining the absorption spectrum of Channelrhodopsins: A case study of the Chimera C1C2

Suliman Adam*, Christian Wiebeler*† and Igor Schapiro*

*Fritz Haber Center for Molecular Dynamics, Institute of Chemistry, The Hebrew University of Jerusalem, Jerusalem 9190401, Israel

†Current Address: Institute for Analytical Chemistry, University of Leipzig, 04103 Leipzig, Germany and Leibniz Institute of Surface Engineering, 04318 Leipzig, Germany

Channelrhodopsin, Absorption Spectrum, Retinal Protein, Rhodopsin, QM/MM

Channelrhodopsins are photosensitive proteins that trigger flagella motion in single cell algae and have been successfully utilized in optogenetic applications. In optogenetics light is used to activate neural cells in living organisms, which can be achieved by exploiting the ion channel signaling of channelrhodopsins. Tailoring channelrhodopsins for such applications includes the tuning of the absorption maximum. In order to establish rational design and to obtain a desired spectral shift, a basic understanding of the absorption spectrum is required. We have studied the chimera C1C2 as a representative of this protein family and the first member with an available crystal structure. For this purpose, we sampled the conformations of C1C2 using QM/MM molecular dynamics, and subjected the resulting snapshots of the trajectory to excitation energy calculations using ADC(2) and simplified TD-DFT. In contrast to previous reports, we found that different hydrogen-bonding networks—involving the retinal protonated Schiff base, the putative counterions E162 and D292 as well as water molecules—had only a small impact on the absorption spectrum. However, in case of deprotonated E162 increasing the distance to the Schiff base hydrogen-bonding partner led to a systematic blue shift. The β-ionone ring rotation was identified as another important contributor. Yet the most important factor was found to be the bond length alternation and bond order alternation that were linearly correlated to the absorption maximum by up to 62 % and 82 %, respectively. We ascribe this novel insight into the structural basis of the absorption spectrum to our enhanced protein setup that includes membrane embedding as well as long and extensive sampling.

Introduction

Channelrhodopsins (ChRs) are light-gated ion channels found in green algae such as *Chlamydomonas reinhardtii*.[1-5] ChRs play a central role in mediating phototaxis by inducing motion in response to the exterior light conditions.[6-8] They are composed of seven transmembrane helices and occur as dimers.[5] A retinal chromophore is bound to ChR via a protonated Schiff base link. Upon light absorption, the retinal protonated Schiff base (RPSB) isomerizes from an all-*trans* to a 13-*cis* form. This starts a photocycle during which cations enter the cell, eventually causing a depolarization of the plasma membrane.[2, 4, 9]

ChRs were the first light-gated cation channels ever discovered and their discovery initiated the field of optogenetics, where light-sensitive ion channels are expressed in cells and are then used to control these altered cells or the organism containing them.[9-15] Channelrhodopsin-1[2] and Channelrhodopsin-2[4] from *C. reinhardtii* (ChR1 and ChR2, respectively) are of particular interest for optogenetics.[16] The native absorption maximum is at 2.60 eV (476 nm) for ChR2,[17-18] whereas ChR1 has a pH-dependent maximum of 2.48–2.64 eV (470–500 nm).[19] To enhance the optogenetic applicability of these ChRs, a molecular level understanding of spectral tuning is desired. One goal is to red-shift the absorption into the optical window between 650 nm and 1350 nm where absorption and scattering inside biological tissue are minimal.[20] Another goal is to engineer significantly shifted ChRs to enable activating two distinct populations by using light of different colors.[21] This can be achieved by modification of the chromophore itself or by alteration of the protein sequence; the latter of which is the reason behind the wide-range absorption spread of naturally occurring retinal proteins: 2.18 eV (568 nm) for bacteriorhodopsin,[22-23] 2.32 eV (534 nm) for green-absorbing proteorhodopsin,[24] 2.11 eV (587 nm) for Sensory Rhodopsin I[25] and

2.55 eV (487 nm) for Sensory Rhodopsin II.[26] Thus, by understanding the role of the retinal environment, we are able to alter it to achieve the desired shift in the absorption maximum.

The ChR1-ChR2 chimera C1C2 (PDB ID: 3UG9[17]) was the first ChR with an available crystal structure and has formed the basis for many theoretical studies on ChRs that focused amongst others on channel opening,[27-28] retinal isomerization,[28-30] or spectral properties.[29, 31-33] C1C2, however, is the result of historical efforts to combine ChR1 and ChR2 in an attempt to obtain chimeras with improved optogenetic properties. C1C2 takes its first five transmembrane helices from ChR1 and its last two from ChR2. It retains many properties of ChR1 that are different from those of ChR2, like the pH-dependence of its absorption maximum.[17, 34] In C1C2, the retinal is attached to K296, and the active-site region contains the counterions E162 and D292, where D292 is also the primary proton acceptor (**Figure 1**).[17, 35] A positively charged lysine residue (K132, **Figure 1**) closes off the active-site region, is responsible for ion selectivity[17] and might form a barrier for ion translocation.[36] E129 (**Figure 1**) is another important residue that affects ion selectivity[17] and prevents ion leakage.[27] Together with E162 and D292, E129 forms part of the central gate, which is the first barrier that prevents water from passing through the channel.[37] The C1C2 crystal structure resolves only a single water molecule inside the active-site region.[17] Yet IR studies indicate that the active site in C1C2 is more hydrated than for other microbial rhodopsins.[38] Theoretical studies using classical molecular dynamics (MD) confirm these findings as well and show a stronger hydration of the protein interior compared to the crystal structure.[33, 39-41] In earlier work,[41] two of the present authors studied the hydration and the effect of E162 protonation. We demonstrated the importance of the hydration for the stability of the Schiff base proton in the dark state of ChR. During these studies, we generated several MD trajectories using a combined quantum mechanical/molecular mechanical (QM/MM) approach.[42-43]

In the present work, we use the QM/MM approach to calculate UV/Vis absorption spectra for C1C2. Because of the large size of the simulated system and its high degree of complexity, multiple minima exist and finding them cannot be done reliably. We, therefore, utilize thermal sampling to understand how the combination of different retinal conformations and environmental effects shape the absorption spectrum in C1C2. In the next section, we will outline the employed methods, before presenting benchmarks of different computational approaches to calculate absorption spectra. Finally, based on our spectral data, we discuss the influence of specific geometric and electronic properties on the retinal absorption maximum.

Methods

Simulation setup

We calculate UV/Vis absorption spectra using the hybrid quantum mechanics/molecular mechanics (QM/MM) model based on the crystal structure of the ChR chimera C1C2 (PDB ID: 3UG9).[17] QM/MM calculations partition the total system into a region of interest, which is described using a quantum mechanical (QM) method, and a larger remaining system, which is described by molecular mechanics (MM), i.e. a classical force field. In recent work,[41] multiple 1 ns QM/MM MD trajectories of dimeric wild-type C1C2 were generated. To this end the self-consistent charge-density-functional tight-binding (SCC-DFTB)[44] method with full third-order extension[45] and 3ob parameters[46] together with Grimme's dispersion correction[47-48] and the CHARMM force field[49] were employed. The generation of the trajectories has been described in more detail in that reference.[41] SCC-DFTB provides a good description of biological systems containing retinal[50-52] and has been utilized in the past to study the impact of the retinal active-site structure on absorption and IR spectra.[53-55] Here, we use four of the previously generated MD trajectories:[41] two with deprotonated E162 and two with protonated. All other amino acid residues are in their standard protonation states, except for E122, E129 and D195, which we model as neutral. We extract 750 equally spaced snapshots from the last 750 ps of each trajectory, and use the respective geometries to compute excitation energies.

Size of the QM Region

Two different QM regions were assessed in the calculation of excitation energies. The QM region that was used during the generation of the trajectories,[41] composed of retinal, the side chains of K296, E129, K132, E162 and D292, and three water molecules (w1, w2, w3) that are located in the Schiff base region is denoted as "Large" (**Figure 1**). To test which impact the size of the QM

region has on the absorption spectrum, we perform additional computations with a minimal QM region consisting only of the RPSB and the K296 side chain (60 atoms in total, denoted as "Small" in **Figure 1**). The latter selection is often used in QM/MM studies of retinal proteins.

In order to cap bonds at the QM/MM boundary, we add hydrogen link atoms to C_β for D292, to C_δ for K132 and to C_γ for E129, E162 and K296. There are 102 and 103 atoms in the "Large" QM region for deprotonated and protonated E162, respectively. The QM treatment is applied to the active site of either monomer 1 or monomer 2 of the C1C2 dimer. [33, 39-41, 56-57] Unless stated otherwise, the "Large" QM region is used.

Calculation of Excitation Energies

We use the QM/MM interface of the AMBER software package[58-59] to prepare the calculation of excitation energies. Each snapshot consists of the QM region and all atoms within 12 Å of the QM region. These atoms surrounding the QM region are treated as point charges and constitute the MM region. The interaction between the QM and the MM regions is described by electrostatic embedding. We employ two different QM methods to compute excitation energies and oscillator strengths. As first method we use the simplified time-dependent density functional theory approach (sTD-DFT) by Grimme and coworkers.[60-62] The sTD-DFT calculations employ the CAM-B3LYP functional[63-65] and the def2-SV(P) basis set.[66] We apply sTD-DFT to compute all excited states of up to 10 eV, and include the first 30 in the analysis. As second QM method we use the more computationally demanding algebraic diagrammatic construction scheme to second order with the resolution-of-identiy (RI) approximation (RI-ADC(2)),[66-69] the cc-pVDZ basis set[70] and the default auxiliary basis set for RI. [71] We apply the RI-ADC(2) approach to a selection of snapshots from the MD trajectory with deprotonated E162 and the QM region located in monomer 1 and determined the first five excitations. This is done to test the agreement between RI-ADC(2) which

compared to high accuracy methods has an accuracy of ~0.2 eV for organic chromophores[72]—and sTD-DFT, which has a much lower computational cost. We perform the sTD-DFT- and RI-ADC(2)-based calculations with the ORCA (version 4.0.1.2)[73-74] and Turbomole (version 7.2)[75-77] software packages, respectively.

For each snapshot, the excitation energies and oscillator strengths of each computed excited state are broadened into Gaussian line shapes with a standard deviation of 0.3 eV. These individual Gaussians are then summed up to obtain the UV/Vis spectrum of a specific snapshot.[78] The individual snapshot spectra are then combined into the final UV/Vis spectra presented here. Similar to an experimental measurement, the location of the maximum is not necessarily identical to the position of the energy of the excitation with the highest oscillator strength. For this reason, we refer to absorption maxima when we discuss the computed spectra.

Results and Discussion

We have performed QM/MM spectral computations on the ChR chimera C1C2 (PDB ID: 3UG9).[17] In this section, we analyze how the selection of the QM region, the choice of the electronic structure method, the hydrogen-bonding network in the active site and the structural factors of the retinal chromophore influence the simulated absorption spectrum of the protein.

Assessment of the Electronic Structure Method

The quantum chemical method for the calculation of excitation energies should balance accuracy and computational cost. Multireference methods have been used widely to study the absorption spectrum in retinal proteins.[30, 79-82] Another commonly used approach is the second-order approximate coupled cluster singles and doubles model (CC2).[32, 83] It has been assessed specifically for excitation energies of organic molecules.[84] However, excitation energy calculations using the methods described above are computationally too demanding for the "Large" QM region (**Figure 1**), considering the computation of 3000 snapshots from thermal sampling. RI-ADC(2) is a computationally less expensive alternative to CC2 that nevertheless provides results of comparable quality. Recently, we have employed RI-ADC(2) to study the absorption spectra of the cyanobacteriochrome Slr1393g3, which enabled us to deduce the origin of its spectral tuning mechanism.[85-86] We found the RI-ADC(2) results to be in close agreement with sTD-DFT, a method which is at least one order of magnitude faster. Therefore, we considered its application to C1C2. To assess the accuracy of sTD-DFT for our system, we have benchmarked sTD-DFT against RI-ADC(2) for 750 snapshots of the MD trajectory with deprotonated E162 and the QM region placed in monomer 1. The absorption maxima are nearly coinciding with 2.34 eV (530 nm) for RI-ADC(2) and 2.35 eV (528 nm) for sTD-DFT (**Figure 2**). However, the RI-ADC(2) absorption band is slightly more extended towards longer wavelengths. We proceeded to

perform all the spectral calculations with sTD-DFT because of its significantly decreased computational cost in comparison to RI-ADC(2), but still similar accuracy. In comparison to the experimental value of 2.60 eV (476 nm),[17-18] the computed maxima are red-shifted by ~0.3 eV.

Several QM/MM studies of C1C2 excitation energy were reported by other groups in the literature (**Table 7**). Within a year after the release of the crystal structure the first two computational studies were published: An approach based on QM/MM geometry optimization and multi-reference MP2 (MR-MP2) with electrostatic embedding was employed by Kamiya et al. yielding 2.91 eV (426 nm).[31] Sneskov et al. optimized the C1C2 geometry as well but calculated QM/MM excitation energies using polarizable embedded RI-CC2, which resulted in 3.00 eV (413 nm).[32] In both works E162 and D292 were assigned to be deprotonated. The possibility of E162 being protonated was investigated by Dokukina and Weingart[29] using several methods for geometry optimization and excitation energy calculation. The best agreement with the experimental absorption maximum, however, was achieved for deprotonated E162 and by combining CASSCF geometry optimization with MS-CASPT2 excitation energies as well as using electrostatic embedding, resulting in 2.59 eV (479 nm).[29] Recently, Olivucci and coworkers employed an automated protocol to setup QM/MM calculation of retinal proteins.[79-80] In contrast to other works, this automated model building provided an MS-CASPT2 excitation energy of 3.33 eV (372 nm)[79] and 2.76 eV (449 nm)[80] depending on whether E162 was deprotonated or protonated. It was therefore concluded that E162 is protonated under conditions for crystallization of C1C2.

Effect of the QM region size

Following the assessment and selection of the electronic structure method we tested the impact of the QM region size on the absorption maximum. The "Large" QM region allows polarization

of the counterions by the RPSB and the residues in the QM region. Polarization of the protein residues surrounding the retinal chromophore can be important for the computation of excitation energies.[32, 54-55, 87] We find that the "Small" QM region (**Figure 1**) yields higher excitation energies compared to the "Large" QM region. Independent of E162 protonation, the difference is 0.08 eV (**Table 1**, **Figure 3**). This small, systematic shift indicates that electrostatic embedding can lead to accurate results without the need to include the counterion complex in the QM description.

The composition of the "Small" and "Large" QM region allows us to break down the effect of the protein environment. We performed further tests by recomputing excitation energies for the "Large" and "Small" QM regions without the MM region, meaning we computed excitation energies of the respective protein adapted geometry in the gas-phase. By removing the protein environment we obtain a reference value for isolated RPSB and the effect of the counterion complex that can be compared to the full environment. Since the "Small" QM region contains only the RPSB, the choice of E162 protonation is not relevant for these calculations when the MM part is excluded (**Figure 1**). Hence, the differences between absorption maxima for trajectory snapshots with either deprotonated or protonated E162 are purely a result of variations in retinal geometry due to the surrounding residues. Indeed, the absorption maxima of 2.14 eV (579 nm) and 2.15 eV (578 nm) for deprotonated and protonated E162, respectively (**Figure 3**), nearly coincide. The results from the calculation of the "Large" QM region without the remaining protein estimate the contribution of the counterion complex to the spectral shift. For the absorption maxima of the "Large" QM region and protonated E162, removal of the MM region has a negligible impact and the maximum is red-shifted by only 0.02 eV to 2.28 eV (543 nm) (**Figure 3**); for deprotonated E162, on the other hand, there is a large blue shift of 0.19 eV to 2.55 eV (485 nm). Buda *et al*. also obtained a blue shift by considering a cluster model for the gas-phase binding pocket of

proteorhodopsin, consisting of RPSB, two negative counterions, a histidine and three water molecules.[57] Experimental action spectra provide further evidence that addition of the negative counterions causes a blue shift to the RPSB absorption.[88]

Adding the remaining protein environment to the "Large" QM region, which already includes the counterion complex, leads to an increase of the absorption by 0.02 eV for the protonated E162 and a decrease by 0.19 eV for the deprotonated E162. The change is smaller compared to the one of adding the counterion complex to the isolated RPSB, that is 0.13 eV and 0.42 eV for the protonated and deprotonated E162, respectively. Hence, the comparison of the gradually increasing system size, i.e. the RPSB in the gas phase, the counterion complex and the entire protein environment, shows that the counterion complex has the largest impact. This can be rationalized on the basis of the point-charge model of retinal proteins.[89-92] This model is based on the fact that a partial, intramolecular charge-transfer in RPSB results in different charge distribution in the ground and excited state. The positive charge in the SB region is reduced in the excited state,[93-94] and therefore a negative counterion will stabilize the ground state more than the excited state, which in turn leads to an increase in the energy gap and a blue shift.

Impact of the E162 protonation state

The calculated C1C2 absorption maximum of the "Large" QM region with deprotonated E162 is 2.36 eV (524 nm), while C1C2 with protonated E162 is red-shifted to 2.30 eV (539 nm) (**Table 1**, **Figure 3**). A similar shift is obtained for the "Small" QM region where E162 protonation causes a change from 2.44 eV (507 nm) to 2.38 eV (520 nm). Experimentally, a decrease in the pH value from 10 to 4 resulted in a 0.07 eV red shift of the C1C2 absorption maximum.[17] This observation, however, cannot be assigned exclusively to the protonation of E162 since other titratable amino acids, like E87 in *Cr*ChR1,[34] might also contribute to the shift. Direct support for the red shift

caused by E162 comes from the action spectrum of the E162Q mutation in C1C2 by Li et al.[95] and from the absorption spectrum of the E162A mutation in Chrimson (E165 in Chrimson) by Urmann et al.[96] Additionally, for ChR from *Volvox carteri* lowering the pH from 7.5 to 4.0 resulted in a red shift of 0.08 eV[97]—almost identical to the 0.07 eV we observe. Theoretical studies by Dokukina and Weingart,[29] as well as Olivucci and coworkers observed a red shift upon E162 protonation.[79-80] Both studies, however, overestimated the shift: the former by 0.15–0.20 eV and the latter even by 0.57 eV. We assume that our improved agreement with the experiment is due to the membrane embedding and thermal sampling. This allows additional water molecules to enter the binding pocket and stabilize the altered interactions of the Schiff base and the counterion.

Hydrogen-Bonding Partners of the Schiff Base

Several studies have shown the Schiff base in ChR to be involved in hydrogen-bonding networks containing the counterions D292/E162 and water molecules.[33, 41, 98-99] Because these interactions can contribute to the opsin shift and because SCC-DFTB is able to model hydrogen-bonding networks with the same quality as full DFT with a medium-sized basis set,[45] we investigated their effect by divding our snapshots into three hydrogen-bonding patterns: The Schiff base hydrogen-bonding with water only (HBw) (**Figure 4**a), the Schiff base hydrogen-bonding with a counterion (HBc) (either D292 or E162, **Figure 4**b), or the Schiff base forming a three-center hydrogen bond with water and either D292 or E162 (HBwc, **Figure 4**c).

The absorption maximum averaged for all snapshots with deprotonated E162 is found at 2.36 eV (524 nm). Our analysis shows an absorption maximum at 2.35 eV (529 nm), 2.37 eV (524 nm) and 2.38 eV (521 nm) for snapshots in the substate HBw, HBc and HBwc, respectively (**Table 1**, **Figure 5**a). The HBw value is red-shifted compared to the average for all snapshots, while the HBc and HBwc values are blue-shifted with respect to the average (**Table 1**, **Figure 5**a). For

protonated E162, the average of all snapshots yields an absorption maximum at 2.30 eV (539 nm) (**Table 1**, **Figure 5**b). While in the substates HBw, HBc and HBwc the absorption maxima lie at 2.30 eV (541 nm), 2.31 eV (536 nm) and 2.33 eV (532 nm), respectively. We see the same behavior as for the deprotonated E162 (**Table 1**, **Figure 5**b). Although, the shifts in the absorption maxima appear to be systematic for different hydrogen bonding patterns, the extent of the shifts is small for both protonation forms (the largest shift is 0.03 eV).

Following the analysis of the spectra for deprotonated and protonated E162 by combining snapshots taken from two trajectories each (one with the QM region in monomer 1 and one in monomer 2), we examine each of the individual trajectories separately. For the trajectory of deprotonated E162 with the QM region in monomer 1, for instance, the differences between the analyzed hydrogen-bonding patterns of the Schiff base are within 0.01 eV and negligible (**Suppl. Table 1**). In the trajectory with the QM region in monomer 2 on the other hand, the average is 2.39 eV (520 nm), while HBw, HBc and HBwc have absorption maxima of 2.34 eV (530 nm), 2.38 eV (522 nm) and 2.40 eV (516 nm), respectively (**Suppl. Table 1**). The differences between the different hydrogen-bonding patterns for the total deprotonated E162 spectra were therefore the result of the contribution from the monomer 2. For protonated E162, the two trajectories also show a slightly different behavior: When the QM region is located in monomer 1, the absorption maximum of HBw, 2.32 eV (536 nm), is blue-shifted by 0.03 eV compared to HBc; whereas with the QM region in monomer 2, HBw has its maximum at 2.28 eV (544 nm) and is red-shifted by 0.10 eV compared to HBc (**Suppl. Table 2**).

As we found the absorption maximum and the hydrogen-bonding partner of the Schiff base to be independent from each other, we proceeded to analyze the dependence of the absorption on the following three parameters: (i) the hydrogen-bonding distance between the Schiff base and its

nearest hydrogen-bonding partner, (ii) the orientation of the β-ionone ring, and (iii) bond length alternation (BLA) and bond order alternation (BOA).

Schiff Base Hydrogen-Bonding Distance

We refined the hydrogen-bonding-based analysis, by dividing the snapshots according to the heavy atom distance between Schiff base nitrogen and its nearest hydrogen-bonding partner—either a water molecule or one of the two counterions. We defined seven ranges between 2.6 Å to 3.3 Å with each range covering 0.1 Å.

For deprotonated E162, the average hydrogen-bonding distance is 2.87 Å and the spectra of the ranges appear to show a correlation between the hydrogen-bonding distance and the location of the absorption maximum. Shorter hydrogen-bonding distances, i.e. stronger hydrogen bonds, correspond to blue-shifted maxima, while longer distances correspond to a red shift (**Figure 7**c). The maxima extend from 2.40 eV (518 nm) for 2.6–2.7 Å until 2.28 eV (545 nm) for 3.2–3.3 Å (**Table 3**). Despite the systematic behavior of the ranges, the Pearson correlation coefficient for the Schiff base hydrogen-bonding distance and the absorption maxima in eV of the individual snapshots was $r = -0.13$, implying at most very weak anti-correlation between these two parameters (**Table 2**).

For protonated E162, the average hydrogen-bonding distance is 2.92 Å and the location of the maxima of the individual ranges appears uncorrelated to the Schiff base hydrogen-bonding distance (**Figure 7**d) with $r = -0.12$ (**Table 2**). The 2.6–2.7 Å range shows a blue shift with respect to the overall average, as was the case for deprotonated E162. In the range of 2.7 Å to 3.3 Å, however, we compute very similar maxima for all ranges (**Table 3**). For both deprotonated and protonated E162, calculating the absorption maximum for snapshots with a Schiff base hydrogen-bonding distance of 2.8–2.9 Å gives the wavelength closest to the average maximum (**Table 3**).

Our analysis suggests that a smaller hydrogen bonding distance contributes to a blue-shifted maximum; even though, we could not find a significant linear correlation between Schiff base hydrogen-bonding distance and absorption maximum (**Table 3**). This result further confirms the aforementioned point-charge model for retinal proteins.

Orientation of the β-Ionone Ring

The retinal β-ionone ring possesses a low barrier for rotation ,[100-101] such that the ring twist for the embedded chromophore is mostly determined by the environment, i.e. the protein–retinal steric interactions.[101-102] According to prior studies, the twist of the β-ionone ring can shift the absorption maximum in retinal proteins.[18, 101, 103] We characterized the ring orientation by the dihedral C_1–C_6–C_7–C_8 at the interface between the β-ionone ring and the retinal π-conjugated chain. We organized the snapshots in 20° intervals covering ring orientations from −35° to 85°. For deprotonated E162, the 25–45° range corresponds best to the average absorption maximum, while for protonated E162, the ranges from 5° to 85° show good agreement with the average. Negative ring twists smaller than −15° result in a blue-shifted maximum of 2.48 eV (501 nm) and 2.41 eV (514 nm) for deprotonated and protonated E162, respectively (**Table 4**). For deprotonated E162 only, ring rotations of more than 45° start inducing blue shifts as well, with the most blue-shifted maximum being 2.52 eV (492 nm) for 65–85°. In general, the ring rotation appears to have a larger impact when E162 is deprotonated.

The individual snapshots themselves are not linearly correlated according to their Pearson coefficient of $r = 0.13$ and $r = −0.07$ for deprotonated and protonated E162, respectively (**Table 2**). Yet, the averages of the ranges imply that twisting the β-ionone ring out of the retinal plane causes a blue shift (**Table 4**, **Figure 7**e–f). For both deprotonated and protonated E162, large twists in either positive or negative direction cause this effect. This observation agrees with theoretical

and experimental studies that link large twists of the β-ionone ring with blue-shifted absorption maxima.[18, 104]

Bond Length Alternation and Bond Order Alternation

The BLA is defined as the difference between the average single bond length and the average double bond length of a π-conjugated system,[105-107] while the BOA is defined as the difference between the average bond order of the single and double bonds.[105] Here, we compute bond orders as defined by Mayer.[108] Both BLA and BOA give us an indication of the level of conjugation of the retinal. The BLA has a big impact on tuning the absorption properties of retinal in its protein environment.[109]

Starting with the BLA, we divided the snapshots into 6 ranges between 0.010 Å and 0.160 Å with each range covering 0.025 Å. Plotting the resulting spectra indicates a correlation between the BLA and the absorption maximum, with smaller BLA, i.e. stronger retinal conjugation, corresponding to a red-shifted maximum (**Figure 7**a–b), analogous to observations made for bacteriorhodospin.[54] For deprotonated E162, the absorption maximum is 2.11 eV (588 nm) for the 0.010–0.035 Å region and 2.71 eV (458 nm) for the 0.135–0.160 Å region, the most red- and blue-shifted bins, respectively. For protonated E162, the maxima are 2.09 eV (593 nm) and 2.51 eV (495 nm) for the two corresponding regions (**Table 5**). We calculated the Pearson correlation coefficients r, and the results confirm BLA and the absorption maximum in eV to be moderately correlated with a coefficient of $r = 0.61$ for deprotonated E162 and 0.54 for protonated E162 (**Table 2**).

Our results show the importance of the BLA as a determinant for the spectral properties of the retinal chromophore, as both protonation states of E162 show similar behavior for BLA dependency, where a change of BLA from ~0.02 Å to ~0.15 Å corresponds to a blue shift of ~0.4–

0.6 eV. The dependence of the absorption maximum on the BLA was also observed in other retinal proteins, suggesting the BLA as a fundamental parameter for spectral tuning.[110-111]

The BLA adds an additional explanation for the blue shift in the absorption maximum, when comparing deprotonated to protonated E162: The distribution of BLAs computed for the snapshot of C1C2 with deprotonated E162 is shifted towards larger BLA values than the distribution in C1C2 with protonated E162. This results in a larger average BLA of 0.062 Å for deprotonated E162 as compared to 0.056 Å for protonated E162. The BLA for deprotonated E162 is comparable to the 0.068 Å value found in a DFT study on retinal in proteorhodopsin,[57] where both counterions are deprotonated. The smaller BLA value from our trajectories can be explained by the fact that DFT methods based on the generalized gradient approximation method, which were used to derive SCC-DFTB, tend to overestimate conjugation, which contributes to a red shift of ~0.1 eV.[54, 109, 112]

The BLA is a good indicator for the electronic structure of a molecule, but since it is computed from geometric properties, the BOA might be better suited for the analysis of optical properties.[105] The BOA is directly computed from electronic properties and behaves more consistently. To sample the impact of the BOA, we generated 6 ranges for BOA of −0.56 to −0.08, where each range covers 0.08. As was the case with the BLA, the BOA shows a clear correlation with the absorption maximum in eV (**Figure 7**c–d), where a stronger conjugation of the retinal, i.e. a less negative BOA, corresponds to a red shift.

The BOA covers a slightly wider spectral range than the BLA (**Table 5**–**Table 6**). The most red-shifted range yields an absorption maximum of 2.05 eV (606 nm) for both protonation states of E162; and the most blue-shifted range absorbs at 2.65 eV (469 nm) for deprotonated E162 and at 2.76 eV (448 nm) for protonated E162 (**Table 6**). When comparing corresponding BOA ranges, C1C2 with deprotonated E162 is red-shifted compared to protonated E162, despite the overall blue

shift, when all snapshots are considered (**Table 6**). However, this can be rationalized by the average BOA values of the deprotonated and protonated E162. The average BOA is −0.45 for deprotonated E162 and −0.39 for protonated E162, i.e. explaining the overall blue shift of the deprotonated E162.

The BOA is highly correlated with the absorption maximum which is reflected in a Pearson correlation coefficient of $r = 0.82$ for deprotonated E162 and of $r = 0.80$ for protonated E162 (**Table 2**). The BOA having a significantly higher correlation than the BLA confirms that the BOA is a more reliable indicator for the absorption maximum and shows how changes in the conjugation greatly affect the width of the band or the absorption maximum.

Conclusions

We have investigated how factors, such as size of the QM region, MM environment, hydrogen-bonding network and retinal geometry influence retinal absorption in ChR C1C2. For this purpose, we have analyzed spectral data derived from QM/MM MD simulations of deprotonated and protonated E162, respectively.

We found that sTD-DFT using the CAM-B3LYP functional yields spectra of sufficient quality at low computational cost. The computed absorption maximum at 2.36 eV (524 nm) is in good agreement with the results of more expensive RI-ADC(2) calculations and is within 0.3 eV of the experimental maximum at 2.60 eV (476 nm) (**Table 1** and **Figure 2**).[17] Employing the efficient sTD-DFT approach enabled us to extend the size of the QM region and to perform more exhaustive thermal sampling. The latter was shown to be important for an accurate description of the retinal absorption spectrum and its broadening at room temperature. This is supported by the observation that small differences in the retinal geometry and protein environment can yield very different absorption maxima for individual snapshots (**Table 4**–**Table 5**).

Furthermore, the embedding of the protein model in a membrane enabled hydration and relaxation of the binding pocket depending on the protonation state of E162. Consequently, the effect of the E162 protonation was significantly smaller than in other static calculations,[29, 79] but in line with the experimental observations at different pH.[17]

In the gas phase we found that inclusion of the counterion complex had the largest contribution to the spectral shift of RPSB (0.3 eV). The remaining protein contributed 0.19 eV in case of deprotonated E162 and much less (0.02 eV) for protonated E162. Comparison of the absorption maxima from calculations with a small and large size QM region indicated that the counterion complex can be excluded from the QM region if electrostatic embedding is used. We conclude that the nature of the retinal–counterion interaction is predominantly electrostatic, as reported in the point-charge model.[89-92]

The absorption maximum for different hydrogen-bonding networks (**Figure 4**) varied within a small range of 0.03 eV (**Table 1**). Further analysis of the monomers revealed that the immediate Schiff base hydrogen-bonding partner and the absorption maximum are independent of each other (**Figure 5** and **Table S1, S2**). Likewise, a study on a homology model of ChR2 by Guo *et al.*[33] found the impact of the hydrogen-bonding networks on the absorption spectrum to be limited and not exceeding 0.06 eV.

We analyzed the hydrogen-bonding distance between the Schiff base nitrogen and its nearest hydrogen-bonding partner irrespective of the type of the hydrogen-bonding network. For deprotonated E162 decreasing the H-bonding distance led to a blue shift; while for protonated E162, we there was no systematic shift. We computed small Pearson correlation coefficients of −0.12 and −0.13 (**Table 2**); hence we conclude that either there are other effects that contribute more strongly to the location of the absorption maximum or that the correlation is nonlinear.

Ultimately, the shift of the retinal absorption maximum is mainly dictated by the electrostatic environment, and we saw evidence that with two negative counterions present a stronger hydrogen bond results in a blue shift of retinal absorption, explaining the overall blue shift caused by having E162 deprotonated (**Table 3**).

For the orientation of the retinal β-ionone ring, we obtained Pearson correlation coefficients close to zero as well (**Table 2**). Large ring torsions in either positive or negative direction resulted in a blue-shifted maximum, but this effect appears to be non-linear, with ring orientations in the range of −15° to 65° only showing slight impacts on the absorption (**Table 4** and **Figure 6**).

The conjugation of the retinal is an important determinant for the excitation energy we investigated. When analyzing the structure of the retinal π-conjugated system, characterized by BLA and BOA (**Figure 7**), we saw a high correlation between BLA and absorption maximum of $r = 0.61$ and $r = 0.54$ for deprotonated and protonated E162, respectively (**Table 2**). As the BLA is a geometric measure, this proved that just the geometry by itself is already a good descriptor of the electronic structure of the retinal. Nevertheless, when working with non-optimized structures, the BLA is less reliable than the BOA,[105] which gives more consistent results. In our study, this is reflected by the very high correlation between BOA and absorption maximum that we found: $r = -0.82$ and $r = -0.80$ for deprotonated and protonated E162, respectively (**Table 2**). This finding is in line with the experimental observation that the absorption spectrum of proteorhodopsin can be tuned by changing the C14–C15 bond length, which was achieved with the L105Q mutation.[110] We, therefore, believe that the conclusions of our C1C2 study can be transferred to other retinal proteins and that they provide a guideline for understanding their spectra and color tuning.
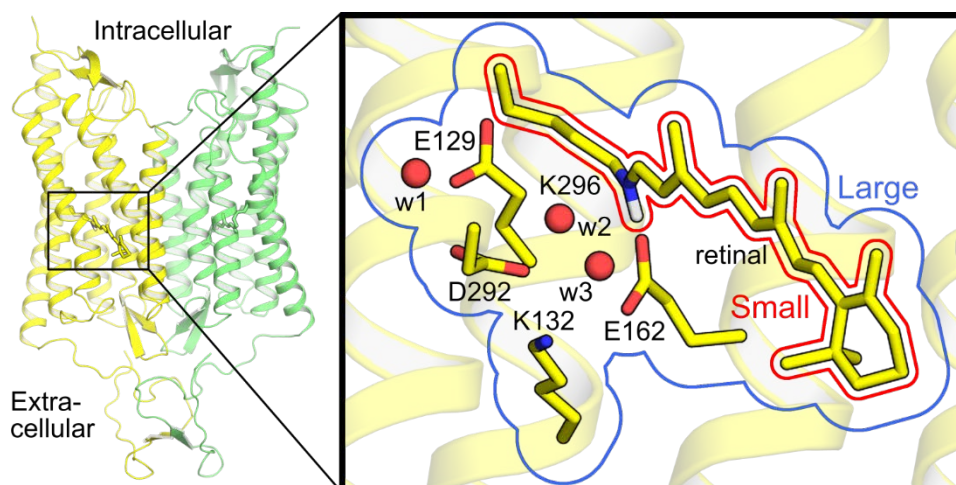
Figures

Figure 1. Channelrhodopsin dimer and zoom-in on the active site, showing the QM regions used for excitation energy calculations. The larger QM region consists of RPSB and K296, the active-site residues E162, D292, E128 and K132 and three nearby water molecules w1, w2 and w3 ("Large", blue). The smaller QM region contains the RPSB and the K296 side chain only ("Small", red).
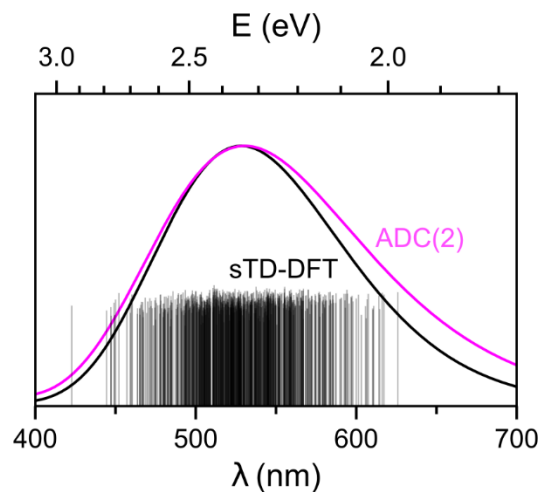
Figure 2. Comparison of sTD-DFT- and RI-ADC(2)-calculated spectra for C1C2 with deprotonated E162. The absorption maximum for RI-ADC(2) (magenta) is 2.34 eV (530 nm) and for sTD-DFT (black) it is 2.35 eV (528 nm). The individual excitations used to generate the sTD-DFT spectrum are shown as black vertical lines for illustrative purposes. The QM region is placed in monomer 1.
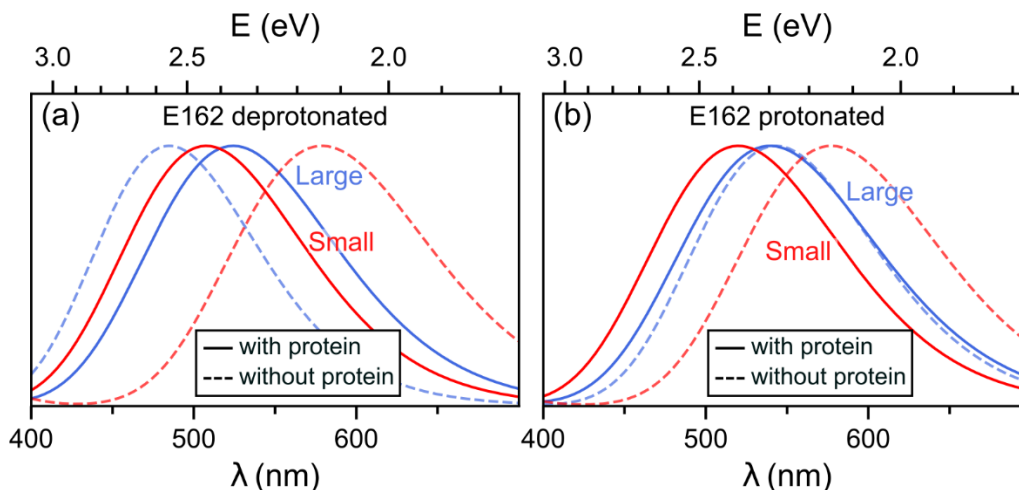
Figure 3. Impact of the retinal environment on the absorption spectrum. Spectra using the "Large" QM region containing RPSB, K296, D292, E162, E129 and three nearby water molecules are shown in blue. Spectra using the "Small" QM region consisting of RPSB with K296 only are shown in red. Solid lines indicate absorption spectra calculated for the respective QM region with electrostatic embedding; while dashes indicate calculations performed for the QM region without any embedding, i.e. *in vacuo*. (a) If E162 is deprotonated, removing the electrostatic embedding from the computations with the "Large" QM region blue-shifts the absorption maximum by 0.19 eV. (b) For protonated E162, the presence of the protein environment does not affect results for the "Large" QM region. Independent of E162 protonation, spectra for the "Small" QM region *in vacuo* are the most red-shifted. With electrostatic embedding the "Small" QM region is 0.08 eV blue-shifted compared to the "Large" QM region.
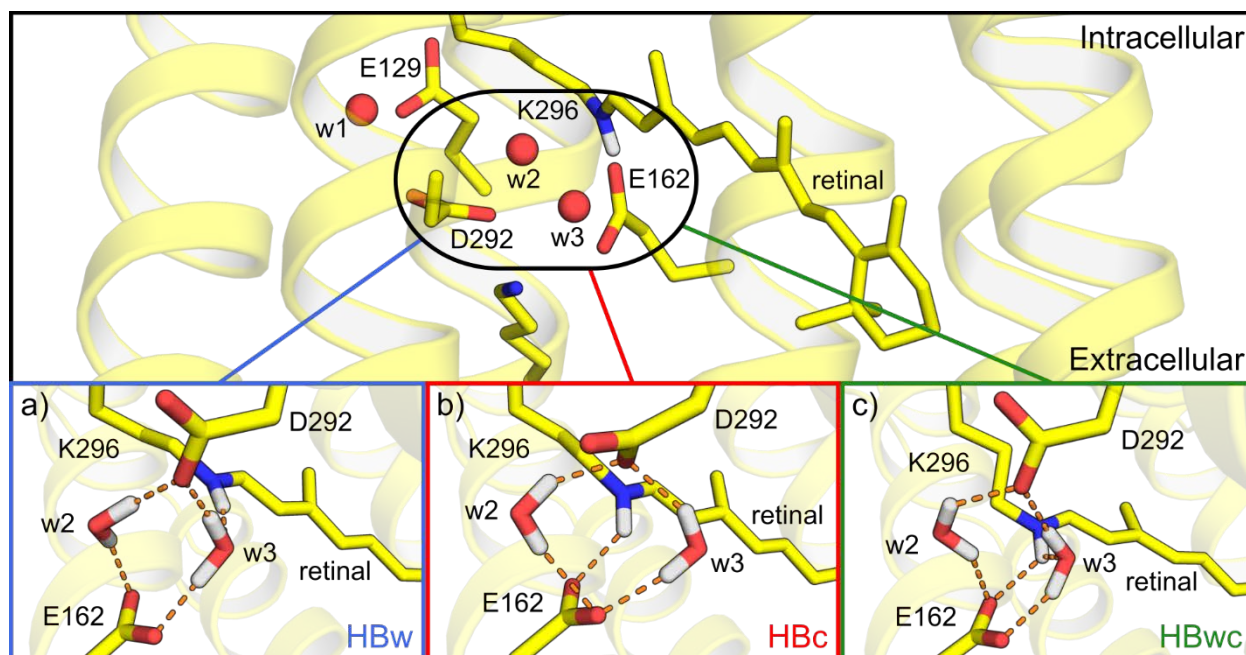
Figure 4. Hydrogen-bonding patterns of the Schiff base nitrogen in C1C2. The top frame shows a close-up of the active-site region with QM residues shown in either stick or spheres representation. (a) The Schiff base is directly hydrogen-bonded to a water molecule (HBw). (b) The Schiff base is hydrogen-bonded to one of the counterions only (HBc). (c) Both a water molecule and one of the counterions are within hydrogen bonding distance of the Schiff base nitrogen (HBwc). Water w2 and w3 are labeled according to Adam and Bondar, Figure 6.[41]
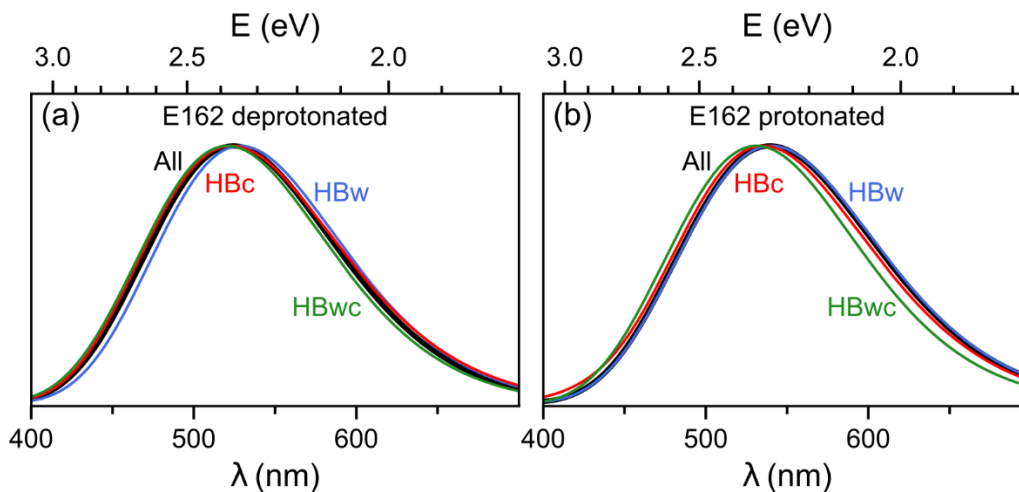
Figure 5. Effect of the hydrogen-bonding pattern on the absorption maximum of C1C2 as computed for deprotonated (a) and protonated E162 (b). The absorption spectrum of the whole simulation is shown in black. The simulation was decomposed into spectra calculated for those snapshots where the Schiff base is interacting directly with water molecules (HBw, blue), only with one of the counterions (HBc, red) or with both, water and one of the counterions (HBwc, green). The impact of a specific hydrogen-bonding pattern on the absorption maximum is small without any systematic shift.
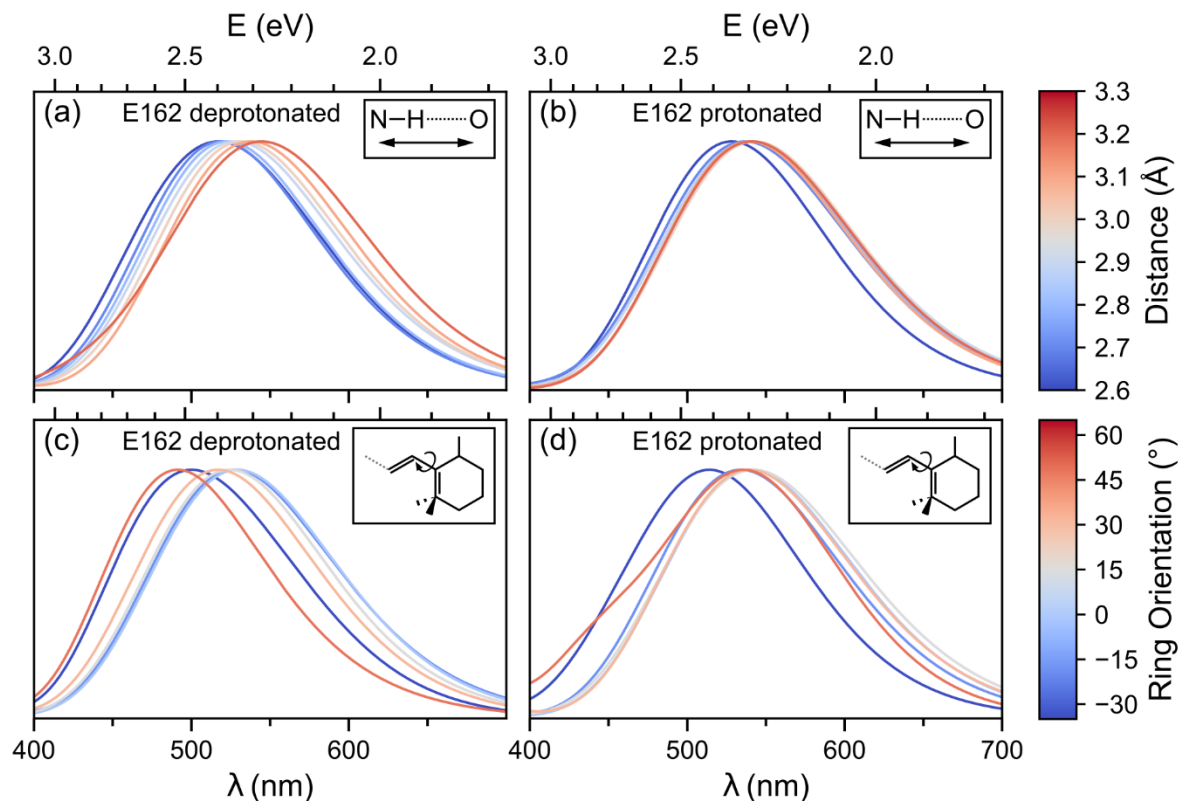
Figure 6. Dissection of the absorption spectra according to the distance between the Schiff base nitrogen and its nearest hydrogen-bonding partner (a–b), and the orientation of the β-ionone ring (c–d). For deprotonated E162, shorter hydrogen-bonding distances result in blue-shifted absorption maxima (a), while for protonated E162, only the 2.6–2.7 Å range is blue-shifted (b). For ring orientations less than −15°, the maximum was shifted to higher energy independent of protonation (c–d).
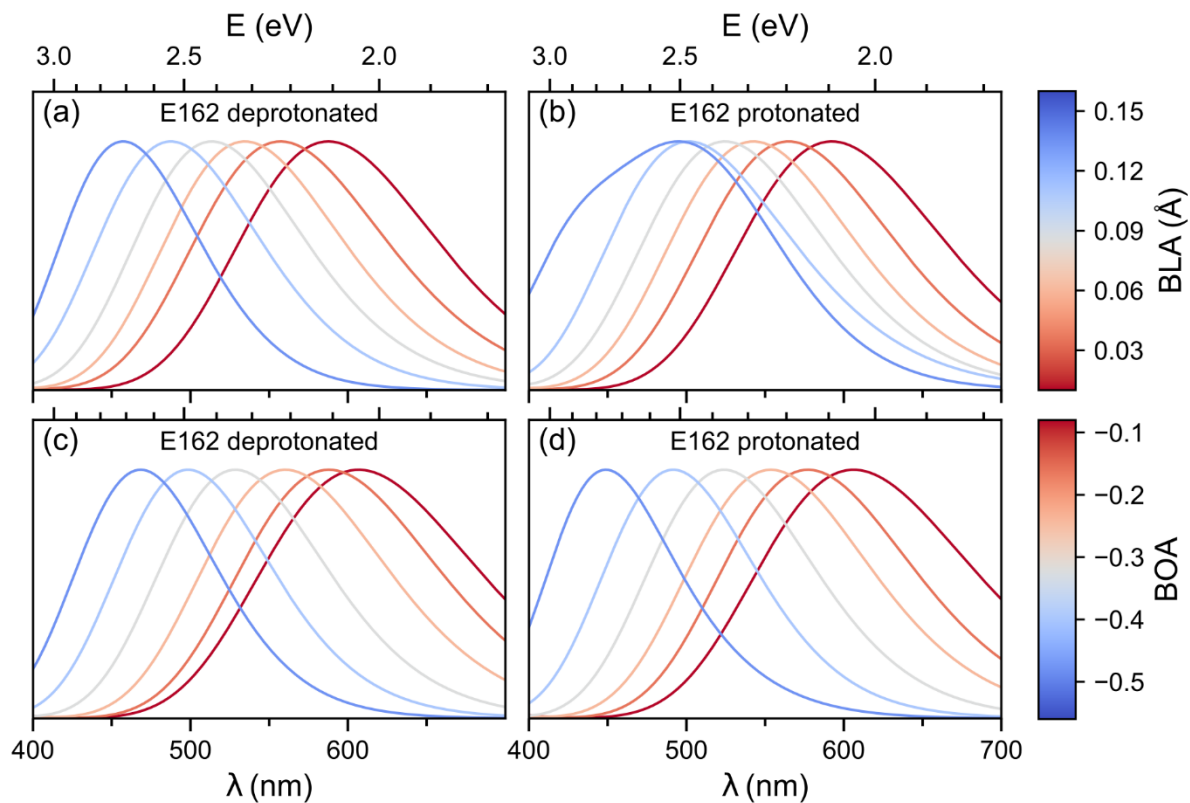
Figure 7. Dissection of the absorption spectra according to bond length alternation (BLA, a–b) and bond order alternation (BOA, c–d). Both BLA and BOA show a high correlation between retinal conjugation and absorption maximum, with a stronger conjugation causing a red shift.

Tables

Table 1. Absorption maxima for different QM regions and hydrogen-bonding patterns of the Schiff base.

QM region	H-bonding pattern[†]	E162 deprotonated		E162 protonated	
		(nm)	(eV)	(nm)	(eV)
Small	All snapshots	507	2.44	520	2.38
	All snapshots[‡]	579	2.14	578	2.15
Large	All snapshots	524	2.36	539	2.30
	All snapshots[‡]	485	2.55	543	2.28
	HBw	529	2.35	541	2.30
	HBc	524	2.37	536	2.31
	HBwc	521	2.38	532	2.33

[†]Hydrogen-bonding patterns according to **Figure 4**.

[‡]Performed for QM region in gas-phase, i.e. without protein embedding.

Table 2. Pearson correlation coefficient *r* for absorption maximum and different parameters.

Parameter	E162 deprotonated.	E162 protonated
H-bonding distance	−0.13	−0.12
Ring orientation	0.13	−0.07
Bond length alternation	0.61	0.54
Bond order alternation	−0.82	−0.80

Table 3. Absorption maxima arranged according to Schiff base hydrogen-bonding distance.

H-bonding Distance (Å)	E162 deprotonated		E162 protonated	
	(nm)	(eV)	(nm)	(eV)
2.6–2.7	518	2.40	529	2.35
2.7–2.8	519	2.39	537	2.31
2.8–2.9	523	2.37	540	2.30
2.9–3.0	529	2.35	541	2.29
3.0–3.1	533	2.33	543	2.28
3.1–3.2	538	2.31	540	2.30
3.2–3.3	545	2.28	541	2.29
Average	524	2.36	539	2.30

Table 4. Absorption maxima arranged according to the orientation of the β-ionone ring.

Ring Orientation (°)	E162 deprotonated		E162 protonated	
	(nm)	(eV)	(nm)	(eV)
−35–−15	501	2.48	514	2.41
−15–5	528	2.35	534	2.32
5–25	529	2.35	541	2.29
25–45	525	2.36	542	2.29
45–65	517	2.40	540	2.30
65–85	492	2.52	536	2.31
Average	524	2.36	539	2.30

Table 5. Absorption maxima arranged according to bond length alternation.

Bond Length Alternation (Å)	E162 deprotonated		E162 protonated	
	(nm)	(eV)	(nm)	(eV)
0.010–0.035	588	2.11	593	2.09
0.035–0.060	558	2.22	565	2.20
0.060–0.085	535	2.32	543	2.28
0.085–0.110	514	2.41	525	2.36
0.110–0.135	488	2.54	502	2.47
0.135–0.160	458	2.71	495	2.51
Average	524	2.36	539	2.30

Table 6. Absorption maxima arranged according to bond order alternation.

Bond Order Alternation	E162 deprotonated		E162 protonated	
	(nm)	(eV)	(nm)	(eV)
−0.16–−0.08	607	2.04	606	2.05
−0.24–−0.16	588	2.11	578	2.15
−0.32–−0.24	561	2.21	554	2.24
−0.40–−0.32	529	2.35	524	2.37
−0.48–−0.40	499	2.49	492	2.52
−0.56–−0.48	469	2.65	448	2.76
Average	524	2.36	539	2.30

Table 7. Overview of QM/MM calculations on C1C2 (PDB ID: 3UG9).[17]

QM Method	QM Region	Embedding	Geometry	Excitation Energy	Ref.
ZINDO/S.	RPSB	electrostatic	Unoptimized MD snapshots[†]	2.42 eV (512 nm)	Ardevol et al.[28]
MS-CASPT2	RPSB	electrostatic	Optimized crystal structure	2.59 eV (479 nm)	Dokukina and Weingart[29]
DFT-MRCI	RPSB	electrostatic	Optimized crystal structure	2.74 eV (452 nm)	Dokukina and Weingart[29]
SORCI	RPSB	electrostatic	Optimized MD snapshots[†]	2.90 eV (428 nm)	Guo et al.[33]
B3LYP	RPSB, K296	polarizable	Optimized crystal structure	2.91 eV (426 nm)	Sneskov et al.[32]
MR-MP2	RPSB	electrostatic	Optimized MD snapshot	2.91 eV (426 nm)	Kamiya et al.[31]
RI-CC2	RPSB, K296	polarizable	Optimized crystal structure	3.00 eV (413 nm)	Sneskov et al.[32]
B3LYP	RPSB, K296	electrostatic	Optimized crystal structure	3.07 eV (404 nm)	Sneskov et al.[32]
OM2/MRCI	RPSB	electrostatic	Unoptimized MD snapshots[†]	3.20 eV (387 nm)	Guo et al.[33]
RI-CC2	RPSB, K296	electrostatic	Optimized crystal structure	3.21 eV (386 nm)	Sneskov et al.[32]
ωPBEh	RPSB, E162, D292	electrostatic	Unoptimized MD snapshots	3.27 eV (380 nm)	Liang et al.[113]

[†]ChR2 homology model based on C1C2
[‡]ChR2 crystal structure (PDB ID: 6EID[114])

ASSOCIATED CONTENT

Supporting Information.

The Supporting Information is available free of charge.

Histograms of the data sampled for the heavy atom distance between the Schiff base nitrogen and its nearest hydrogen-bonding partner (Figures S1); Histograms of the data sampled for the orientation of the β-ionone ring (Figure S2); Absorption maxima for different QM regions and hydrogen-bonding patterns of the Schiff base with E162 deprotonated (Table S1); Absorption maxima for different QM regions and hydrogen-bonding patterns of the Schiff base with E162 protonated (Table S2). (PDF)

AUTHOR INFORMATION

Corresponding Author

*E-mail: igor.schapiro@mail.huji.ac.il

Author Contributions

S.A. carried out the computations and data analysis, drafted the manuscript and designed the figures. C.W. performed preliminary calculations. I.S. supervised the project. C.W. and I.S. contributed to the interpretation of the results and worked on the manuscript. All authors commented on the manuscript.

ORCID

Suliman Adam: 0000-0002-0891-5008

Christian Wiebeler: 0000-0003-1286-0860

Igor Schapiro: 0000-0001-8536-6869

Notes

The authors declare no competing financial interest.

REFERENCES

1.   Beckmann, M.; Hegemann, P., In vitro identification of rhodopsin in the green alga Chlamydomonas. *Biochemistry* **1991,** *30* (15), 3692-3697.

2.   Nagel, G.; Ollig, D.; Fuhrmann, M.; Kateriya, S.; Musti, A. M.; Bamberg, E.; Hegemann, P., Channelrhodopsin-1: a light-gated proton channel in green algae. *Science* **2002,** *296* (5577), 2395-8.

3.   Ehlenbeck, S.; Gradmann, D.; Braun, F.-J.; Hegemann, P., Evidence for a Light-Induced

H+ Conductance in the Eye of the Green Alga Chlamydomonas reinhardtii. *Biophysical Journal*

2002, *82* (2), 740-751.

4.   Nagel, G.; Szellas, T.; Huhn, W.; Kateriya, S.; Adeishvili, N.; Berthold, P.; Ollig, D.;

Hegemann, P.; Bamberg, E., Channelrhodopsin-2, a directly light-gated cation-selective

membrane channel. *Proc Natl Acad Sci U S A* **2003,** *100* (24), 13940-5.

5.   Muller, M.; Bamann, C.; Bamberg, E.; Kuhlbrandt, W., Projection structure of

channelrhodopsin-2 at 6 A resolution by electron crystallography. *J Mol Biol* **2011,** *414* (1), 86-

95.

6.   Sineshchekov, O. A.; Litvin, F. F.; Keszthelyi, L., Two components of photoreceptor

potential in phototaxis of the flagellated green alga Haematococcus pluvialis. *Biophysical*

Journal **1990,** *57* (1), 33-39.

7.   Holland, E. M.; Harz, H.; Uhl, R.; Hegemann, P., Control of phobic behavioral responses

by rhodopsin-induced photocurrents in Chlamydomonas. *Biophysical Journal* **1997,** *73* (3),

1395-1401.

8.   Sineshchekov, O. A.; Govorunova, E. G., Rhodopsin-mediated photosensing in green

flagellated algae. *Trends in Plant Science* **1999,** *4* (2), 58-63.

9.   Berthold, P.; Tsunoda, S. P.; Ernst, O. P.; Mages, W.; Gradmann, D.; Hegemann, P.,

Channelrhodopsin-1 initiates phototaxis and photophobic responses in chlamydomonas by

immediate light-induced depolarization. *The Plant cell* **2008,** *20* (6), 1665-77.

10.   Boyden, E. S.; Zhang, F.; Bamberg, E.; Nagel, G.; Deisseroth, K., Millisecond-timescale, genetically targeted optical control of neural activity. *Nature neuroscience* **2005,** *8* (9), 1263-8.

11.   Li, X.; Gutierrez, D. V.; Hanson, M. G.; Han, J.; Mark, M. D.; Chiel, H.; Hegemann, P.; Landmesser, L. T.; Herlitze, S., Fast noninvasive activation and inhibition of neural and network activity by vertebrate rhodopsin and green algae channelrhodopsin. *Proc Natl Acad Sci U S A* **2005,** *102* (49), 17816-21.

12.   Yizhar, O.; Fenno, L. E.; Davidson, T. J.; Mogri, M.; Deisseroth, K., Optogenetics in neural systems. *Neuron* **2011,** *71* (1), 9-34.

13.   Mace, E.; Caplette, R.; Marre, O.; Sengupta, A.; Chaffiol, A.; Barbe, P.; Desrosiers, M.; Bamberg, E.; Sahel, J. A.; Picaud, S.; Duebel, J.; Dalkara, D., Targeting channelrhodopsin-2 to ON-bipolar cells with vitreally administered AAV Restores ON and OFF visual responses in blind mice. *Molecular therapy : the journal of the American Society of Gene Therapy* **2015,** *23* (1), 7-16.

14.   Bruegmann, T.; van Bremen, T.; Vogt, C. C.; Send, T.; Fleischmann, B. K.; Sasse, P., Optogenetic control of contractile function in skeletal muscle. *Nat Commun* **2015,** *6*, 7153.

15.   Lorenz-Fonfria, V. A.; Heberle, J., Channelrhodopsin unchained: structure and mechanism of a light-gated cation channel. *Biochimica et biophysica acta* **2014,** *1837* (5), 626-42.

16.   Zhang, F.; Vierock, J.; Yizhar, O.; Fenno, L. E.; Tsunoda, S.; Kianianmomeni, A.; Prigge, M.; Berndt, A.; Cushman, J.; Polle, J.; Magnuson, J.; Hegemann, P.; Deisseroth, K., The microbial opsin family of optogenetic tools. *Cell* **2011,** *147* (7), 1446-57.

17.   Kato, H. E.; Zhang, F.; Yizhar, O.; Ramakrishnan, C.; Nishizawa, T.; Hirata, K.; Ito, J.; Aita, Y.; Tsukazaki, T.; Hayashi, S.; Hegemann, P.; Maturana, A. D.; Ishitani, R.; Deisseroth, K.; Nureki, O., Crystal structure of the channelrhodopsin light-gated cation channel. *Nature* **2012,** *482* (7385), 369-74.

18.   Kato, H. E.; Kamiya, M.; Sugo, S.; Ito, J.; Taniguchi, R.; Orito, A.; Hirata, K.; Inutsuka, A.; Yamanaka, A.; Maturana, A. D.; Ishitani, R.; Sudo, Y.; Hayashi, S.; Nureki, O., Atomistic design of microbial opsin-based blue-shifted optogenetics tools. *Nat Commun* **2015,** *6*, 7177.

19.   Ritter, E.; Stehfest, K.; Berndt, A.; Hegemann, P.; Bartl, F. J., Monitoring light-induced structural changes of Channelrhodopsin-2 by UV-visible and Fourier transform infrared spectroscopy. *J Biol Chem* **2008,** *283* (50), 35033-41.

20.   Smith, A. M.; Mancini, M. C.; Nie, S., Bioimaging: second window for in vivo imaging. *Nat Nanotechnol* **2009,** *4* (11), 710-1.

21.   Fenno, L.; Yizhar, O.; Deisseroth, K., The development and application of optogenetics. *Annual review of neuroscience* **2011,** *34*, 389-412.

22.   Oesterhelt, D.; Stoeckenius, W., Rhodopsin-like Protein from the Purple Membrane of Halobacterium halobium. *Nature New Biology* **1971,** *233* (39), 149-152.

23.   Birge, R. R.; Zhang, C. F., Two-photon double resonance spectroscopy of bacteriorhodopsin. Assignment of the electronic and dipolar properties of the low-lying 1A*−g-like and 1B*+u-like π, π* states. *The Journal of Chemical Physics* **1990,** *92* (12), 7178-7195.

24.	Gushchin, I.; Chervakov, P.; Kuzmichev, P.; Popov, A. N.; Round, E.; Borshchevskiy, V.; Ishchenko, A.; Petrovskaya, L.; Chupin, V.; Dolgikh, D. A.; Arseniev, A. S.; Kirpichnikov, M.; Gordeliy, V., Structural insights into the proton pumping by unusual proteorhodopsin from nonmarine bacteria. *Proc Natl Acad Sci U S A* **2013,** *110* (31), 12631-6.

25.	Spudich, J. L.; Bogomolni, R. A., Mechanism of colour discrimination by a bacterial sensory rhodopsin. *Nature* **1984,** *312* (5994), 509-513.

26.	Takahashi, T.; Yan, B.; Mazur, P.; Derguini, F.; Nakanishi, K.; Spudich, J. L., Color regulation in the archaebacterial phototaxis receptor phoborhodopsin (sensory rhodopsin II). *Biochemistry* **2002,** *29* (36), 8467-8474.

27.	Takemoto, M.; Kato, H. E.; Koyama, M.; Ito, J.; Kamiya, M.; Hayashi, S.; Maturana, A. D.; Deisseroth, K.; Ishitani, R.; Nureki, O., Molecular Dynamics of Channelrhodopsin at the Early Stages of Channel Opening. *PLoS One* **2015,** *10* (6), e0131094.

28.	Ardevol, A.; Hummer, G., Retinal isomerization and water-pore formation in channelrhodopsin-2. *Proc Natl Acad Sci U S A* **2018,** *115* (14), 3557-3562.

29.	Dokukina, I.; Weingart, O., Spectral properties and isomerisation path of retinal in C1C2 channelrhodopsin. *Physical chemistry chemical physics : PCCP* **2015,** *17* (38), 25142-50.

30.	Guo, Y.; Wolff, F. E.; Schapiro, I.; Elstner, M.; Marazzi, M., Different hydrogen bonding environments of the retinal protonated Schiff base control the photoisomerization in channelrhodopsin-2. *Physical chemistry chemical physics : PCCP* **2018,** *20* (43), 27501-27509.

31.   Kamiya, M.; Kato, H. E.; Ishitani, R.; Nureki, O.; Hayashi, S., Structural and spectral characterizations of C1C2 channelrhodopsin and its mutants by molecular simulations. *Chemical Physics Letters* **2013,** *556*, 266-271.

32.   Sneskov, K.; Olsen, J. M.; Schwabe, T.; Hattig, C.; Christiansen, O.; Kongsted, J., Computational screening of one- and two-photon spectrally tuned channelrhodopsin mutants. *Physical chemistry chemical physics : PCCP* **2013,** *15* (20), 7567-76.

33.   Guo, Y.; Beyle, F. E.; Bold, B. M.; Watanabe, H. C.; Koslowski, A.; Thiel, W.; Hegemann, P.; Marazzi, M.; Elstner, M., Active site structure and absorption spectrum of channelrhodopsin-2 wild-type and C128T mutant. *Chemical Science* **2016,** *7* (6), 3879-3891.

34.   Tsunoda, S. P.; Hegemann, P., Glu 87 of channelrhodopsin-1 causes pH-dependent color tuning and fast photocurrent inactivation. *Photochem Photobiol* **2009,** *85* (2), 564-9.

35.   Lorenz-Fonfria, V. A.; Resler, T.; Krause, N.; Nack, M.; Gossing, M.; Fischer von Mollard, G.; Bamann, C.; Bamberg, E.; Schlesinger, R.; Heberle, J., Transient protonation changes in channelrhodopsin-2 and their relevance to channel gating. *Proc Natl Acad Sci U S A* **2013,** *110* (14), E1273-81.

36.   Richards, R.; Dempski, R. E., Adjacent channelrhodopsin-2 residues within transmembranes 2 and 7 regulate cation selectivity and distribution of the two open states. *J Biol Chem* **2017,** *292* (18), 7314-7326.

37.   Wietek, J.; Wiegert, J. S.; Adeishvili, N.; Schneider, F.; Watanabe, H.; Tsunoda, S. P.; Vogt, A.; Elstner, M.; Oertner, T. G.; Hegemann, P., Conversion of channelrhodopsin into a light-gated chloride channel. *Science* **2014,** *344* (6182), 409-12.

38.   Ito, S.; Kato, H. E.; Taniguchi, R.; Iwata, T.; Nureki, O.; Kandori, H., Water-containing hydrogen-bonding network in the active center of channelrhodopsin. *J Am Chem Soc* **2014,** *136* (9), 3475-82.

39.   Watanabe, H. C.; Welke, K.; Schneider, F.; Tsunoda, S.; Zhang, F.; Deisseroth, K.; Hegemann, P.; Elstner, M., Structural model of channelrhodopsin. *J Biol Chem* **2012,** *287* (10), 7456-66.

40.   Watanabe, H. C.; Welke, K.; Sindhikara, D. J.; Hegemann, P.; Elstner, M., Towards an understanding of channelrhodopsin function: simulations lead to novel insights of the channel mechanism. *J Mol Biol* **2013,** *425* (10), 1795-814.

41.   Adam, S.; Bondar, A. N., Mechanism by which water and protein electrostatic interactions control proton transfer at the active site of channelrhodopsin. *PLoS One* **2018,** *13* (8), e0201298.

42.   Warshel, A.; Levitt, M., Theoretical studies of enzymic reactions: Dielectric, electrostatic and steric stabilization of the carbonium ion in the reaction of lysozyme. *Journal of Molecular Biology* **1976,** *103* (2), 227-249.

43.   Senn, H. M.; Thiel, W., QM/MM methods for biomolecular systems. *Angewandte Chemie* **2009,** *48* (7), 1198-229.

44.   Elstner, M.; Porezag, D.; Jungnickel, G.; Elsner, J.; Haugk, M.; Frauenheim, T.; Suhai, S.; Seifert, G., Self-consistent-charge density-functional tight-binding method for simulations of complex materials properties. *Physical Review B* **1998,** *58* (11), 7260-7268.

45.   Gaus, M.; Cui, Q.; Elstner, M., DFTB3: Extension of the self-consistent-charge density-functional tight-binding method (SCC-DFTB). *J Chem Theory Comput* **2012,** *7* (4), 931-948.

46.   Gaus, M.; Goez, A.; Elstner, M., Parametrization and Benchmark of DFTB3 for Organic Molecules. *J Chem Theory Comput* **2013,** *9* (1), 338-54.

47.   Grimme, S.; Antony, J.; Ehrlich, S.; Krieg, H., A consistent and accurate ab initio parametrization of density functional dispersion correction (DFT-D) for the 94 elements H-Pu. *J Chem Phys* **2010,** *132* (15), 154104.

48.   Grimme, S.; Ehrlich, S.; Goerigk, L., Effect of the damping function in dispersion corrected density functional theory. *J Comput Chem* **2011,** *32* (7), 1456-65.

49.   Brooks, B. R.; Bruccoleri, R. E.; Olafson, B. D.; States, D. J.; Swaminathan, S.; Karplus, M., CHARMM: A program for macromolecular energy, minimization, and dynamics calculations. *Journal of Computational Chemistry* **1983,** *4* (2), 187-217.

50.   Elstner, M., The SCC-DFTB method and its application to biological systems. *Theoretical Chemistry Accounts* **2005,** *116* (1-3), 316-325.

51.   Bondar, A. N.; Suhai, S.; Fischer, S.; Smith, J. C.; Elstner, M., Suppression of the back proton-transfer from Asp85 to the retinal Schiff base in bacteriorhodopsin: a theoretical analysis of structural elements. *Journal of structural biology* **2007,** *157* (3), 454-69.

52.   Zhou, H.; Tajkhorshid, E.; Frauenheim, T.; Suhai, S.; Elstner, M., Performance of the AM1, PM3, and SCC-DFTB methods in the study of conjugated Schiff base molecules. *Chemical Physics* **2002,** *277* (2), 91-103.

53.   Welke, K.; Watanabe, H. C.; Wolter, T.; Gaus, M.; Elstner, M., QM/MM simulations of vibrational spectra of bacteriorhodopsin and channelrhodopsin-2. *Physical chemistry chemical physics : PCCP* **2013,** *15* (18), 6651-9.

54.   Wolter, T.; Welke, K.; Phatak, P.; Bondar, A. N.; Elstner, M., Excitation energies of a water-bridged twisted retinal structure in the bacteriorhodopsin proton pump: a theoretical investigation. *Physical chemistry chemical physics : PCCP* **2013,** *15* (30), 12582-90.

55.   Wolter, T.; Elstner, M.; Fischer, S.; Smith, J. C.; Bondar, A. N., Mechanism by which untwisting of retinal leads to productive bacteriorhodopsin photocycle states. *The journal of physical chemistry. B* **2015,** *119* (6), 2229-40.

56.   Valsson, O.; Campomanes, P.; Tavernelli, I.; Rothlisberger, U.; Filippi, C., Rhodopsin Absorption from First Principles: Bypassing Common Pitfalls. *J Chem Theory Comput* **2013,** *9* (5), 2441-54.

57.   Buda, F.; Keijer, T.; Ganapathy, S.; de Grip, W. J., A Quantum-mechanical Study of the Binding Pocket of Proteorhodopsin: Absorption and Vibrational Spectra Modulated by Analogue Chromophores. *Photochem Photobiol* **2017,** *93* (6), 1399-1406.

58.   Gotz, A. W.; Clark, M. A.; Walker, R. C., An extensible interface for QM/MM molecular dynamics simulations with AMBER. *J Comput Chem* **2014,** *35* (2), 95-108.

59.   Case, D. A.; Betz, R. M.; Cerutti, D. S.; Cheatham, I., T. E.; Darden, T. A.; Duke, R. E.; Giese, T. J.; Gohlke, H.; Goetz, A. W.; Homeyer, N.; Izadi, S.; Janowski, P.; Kaus, J.; Kovalenko, A.; Lee, T. S.; LeGrand, S.; Li, P.; Lin, C.; Luchko, T.; Luo, R.; Madej, B.; Mermelstein, D.; Merz, K. M.; Monard, G.; Nguyen, H.; Nguyen, H. T.; Omelyan, I.; Onufriev,

A.; Roe, D. R.; Roitberg, A.; Sagui, C.; Simmerling, C. L.; Botello-Smith, W. M.; Swails, J.; Walker, R. C.; Wang, J.; Wolf, R. M.; Wu, X.; Xiao, L.; Kollman, P. A. *AMBER 2016*, University of California, San Francisco, 2016.

60.   Bannwarth, C.; Grimme, S., A simplified time-dependent density functional theory approach for electronic ultraviolet and circular dichroism spectra of very large molecules. *Computational and Theoretical Chemistry* **2014,** *1040-1041*, 45-53.

61.   Grimme, S., A simplified Tamm-Dancoff density functional approach for the electronic excitation spectra of very large molecules. *J Chem Phys* **2013,** *138* (24), 244104.

62.   Risthaus, T.; Hansen, A.; Grimme, S., Excited states using the simplified Tamm-Dancoff-Approach for range-separated hybrid density functionals: development and application. *Physical chemistry chemical physics : PCCP* **2014,** *16* (28), 14408-19.

63.   Yanai, T.; Tew, D. P.; Handy, N. C., A new hybrid exchange–correlation functional using the Coulomb-attenuating method (CAM-B3LYP). *Chemical Physics Letters* **2004,** *393* (1-3), 51-57.

64.   Becke, A. D., Density-functional exchange-energy approximation with correct asymptotic behavior. *Physical Review A* **1988,** *38* (6), 3098-3100.

65.   Lee, C.; Yang, W.; Parr, R. G., Development of the Colle-Salvetti correlation-energy formula into a functional of the electron density. *Physical Review B* **1988,** *37* (2), 785-789.

66.   Weigend, F.; Ahlrichs, R., Balanced basis sets of split valence, triple zeta valence and quadruple zeta valence quality for H to Rn: Design and assessment of accuracy. *Physical chemistry chemical physics : PCCP* **2005,** *7* (18), 3297-305.

67.   Hättig, C., Structure Optimizations for Excited States with Correlated Second-Order Methods: CC2 and ADC(2). *Advances in Quantum Chemistry* **2005,** *50*, 37-60.

68.   Schirmer, J., Beyond the random-phase approximation: A new approximation scheme for the polarization propagator. *Physical Review A* **1982,** *26* (5), 2395-2416.

69.   Trofimov, A. B.; Schirmer, J., An efficient polarization propagator approach to valence electron excitation spectra. *Journal of Physics B: Atomic, Molecular and Optical Physics* **1995,** *28* (12), 2299-2324.

70.   Dunning, T. H., Gaussian basis sets for use in correlated molecular calculations. I. The atoms boron through neon and hydrogen. *The Journal of Chemical Physics* **1989,** *90* (2), 1007-1023.

71.   Weigend, F.; Köhn, A.; Hättig, C., Efficient use of the correlation consistent basis sets in resolution of the identity MP2 calculations. *The Journal of Chemical Physics* **2002,** *116* (8), 3175-3183.

72.   Harbach, P. H.; Wormit, M.; Dreuw, A., The third-order algebraic diagrammatic construction method (ADC(3)) for the polarization propagator for closed-shell molecules: efficient implementation and benchmarking. *J Chem Phys* **2014,** *141* (6), 064113.

73.   Neese, F., The ORCA program system. *Wiley Interdisciplinary Reviews: Computational Molecular Science* **2012,** *2* (1), 73-78.

74.   Neese, F., Software update: the ORCA program system, version 4.0. *Wiley Interdisciplinary Reviews: Computational Molecular Science* **2018,** *8* (1), e1327.

75.   GmbH, F. K. *TURBOMOLE Version 7.2*, TURBOMOLE GmbH: 2017.

76.   Furche, F.; Ahlrichs, R.; Hättig, C.; Klopper, W.; Sierka, M.; Weigend, F., Turbomole. *Wiley Interdisciplinary Reviews: Computational Molecular Science* **2014,** *4* (2), 91-100.

77.   Hättig, C.; Hellweg, A.; Kohn, A., Distributed memory parallel implementation of energies and gradients for second-order Moller-Plesset perturbation theory with the resolution-of-the-identity approximation. *Physical chemistry chemical physics : PCCP* **2006,** *8* (10), 1159-69.

78.   Creating UV/Visible Plots from the Results of Excited States Calculations. https://gaussian.com/uvvisplot/ (accessed 30/07/2019).

79.   Melaccio, F.; Del Carmen Marin, M.; Valentini, A.; Montisci, F.; Rinaldi, S.; Cherubini, M.; Yang, X.; Kato, Y.; Stenrup, M.; Orozco-Gonzalez, Y.; Ferre, N.; Luk, H. L.; Kandori, H.; Olivucci, M., Toward Automatic Rhodopsin Modeling as a Tool for High-Throughput Computational Photobiology. *J Chem Theory Comput* **2016,** *12* (12), 6020-6034.

80.   Pedraza-Gonzalez, L.; De Vico, L.; Mari, N. M.; Fanelli, F.; Olivucci, M., a-ARM: Automatic Rhodopsin Modeling with Chromophore Cavity Generation, Ionization State Selection, and External Counterion Placement. *J Chem Theory Comput* **2019,** *15* (5), 3134-3152.

81.   Pieri, E.; Ledentu, V.; Sahlin, M.; Dehez, F.; Olivucci, M.; Ferre, N., CpHMD-Then-QM/MM Identification of the Amino Acids Responsible for the Anabaena Sensory Rhodopsin pH-Dependent Electronic Absorption Spectrum. *J Chem Theory Comput* **2019,** *15* (8), 4535-4546.

82.   Lee, C.; Sekharan, S.; Mertz, B., Theoretical Insights into the Mechanism of Wavelength Regulation in Blue-Absorbing Proteorhodopsin. *The journal of physical chemistry. B* **2019,** *123* (50), 10631-10641.

83.   Suomivuori, C. M.; Lang, L.; Sundholm, D.; Gamiz-Hernandez, A. P.; Kaila, V. R., Tuning the Protein-Induced Absorption Shifts of Retinal in Engineered Rhodopsin Mimics. *Chemistry* **2016,** *22* (24), 8254-61.

84.   Schreiber, M.; Silva-Junior, M. R.; Sauer, S. P.; Thiel, W., Benchmarks for electronically excited states: CASPT2, CC2, CCSD, and CC3. *J Chem Phys* **2008,** *128* (13), 134110.

85.   Wiebeler, C.; Rao, A. G.; Gartner, W.; Schapiro, I., The Effective Conjugation Length Is Responsible for the Red/Green Spectral Tuning in the Cyanobacteriochrome Slr1393g3. *Angewandte Chemie* **2019,** *58* (7), 1934-1938.

86.   Wiebeler, C.; Schapiro, I., QM/MM Benchmarking of Cyanobacteriochrome Slr1393g3 Absorption Spectra. *Molecules* **2019,** *24* (9).

87.   Wanko, M.; Hoffmann, M.; Frauenheim, T.; Elstner, M., Effect of polarization on the opsin shift in rhodopsins. 1. A combined QM/QM/MM model for bacteriorhodopsin and pharaonis sensory rhodopsin II. *The journal of physical chemistry. B* **2008,** *112* (37), 11462-7.

88.   Toker, Y.; Langeland, J.; Gruber, E.; Kjær, C.; Nielsen, S. B.; Andersen, L. H.; Borin, V. A.; Schapiro, I., Counterion-controlled spectral tuning of the protonated Schiff-base retinal. *Physical Review A* **2018,** *98* (4).

89.   Honig, B.; Dinur, U.; Nakanishi, K.; Balogh-Nair, V.; Gawinowicz, M. A.; Arnaboldi, M.; Motto, M. G., An external point-charge model for wavelength regulation in visual pigments. *Journal of the American Chemical Society* **1979,** *101* (23), 7084-7086.

90.   Nakanishi, K.; Balogh-Nair, V.; Arnaboldi, M.; Tsujimoto, K.; Honig, B., An external point-charge model for bacteriorhodopsin to account for its purple color. *Journal of the American Chemical Society* **1980,** *102* (27), 7945-7947.

91.   Warshel, A., Charge stabilization mechanism in the visual and purple membrane pigments. *Proc Natl Acad Sci U S A* **1978,** *75* (6), 2558-62.

92.   Motto, M. G.; Sheves, M.; Tsujimoto, K.; Balogh-Nair, V.; Nakanishi, K., Opsin shifts in bovine rhodopsin and bacteriorhodopsin. Comparison of two external point-charge models. *Journal of the American Chemical Society* **1980,** *102* (27), 7947-7949.

93.   Orozco-Gonzalez, Y.; Kabir, M. P.; Gozem, S., Electrostatic Spectral Tuning Maps for Biological Chromophores. *The journal of physical chemistry. B* **2019,** *123* (23), 4813-4824.

94.   Melaccio, F.; Ferre, N.; Olivucci, M., Quantum chemical modeling of rhodopsin mutants displaying switchable colors. *Physical chemistry chemical physics : PCCP* **2012,** *14* (36), 12485-95.

95.   Li, H.; Govorunova, E. G.; Sineshchekov, O. A.; Spudich, J. L., Role of a helix B lysine residue in the photoactive site in channelrhodopsins. *Biophys J* **2014,** *106* (8), 1607-17.

96.   Urmann, D.; Lorenz, C.; Linker, S. M.; Braun, M.; Wachtveitl, J.; Bamann, C., Photochemical Properties of the Red-shifted Channelrhodopsin Chrimson. *Photochem Photobiol* **2017,** *93* (3), 782-795.

97.   Ernst, O. P.; Murcia, P. A. S.; Daldrop, P.; Tsunoda, S. P.; Kateriya, S.; Hegemann, P., Photoactivation of Channelrhodopsin. *Journal of Biological Chemistry* **2008,** *283* (3), 1637-1643.

98.   VanGordon, M. R.; Gyawali, G.; Rick, S. W.; Rempe, S. B., Atomistic Study of Intramolecular Interactions in the Closed-State Channelrhodopsin Chimera, C1C2. *Biophys J* **2017,** *112* (5), 943-952.

99.   Dokukina, I.; Nenov, A.; Garavelli, M.; Marian, C. M.; Weingart, O., QM/MM Photodynamics of Retinal in the Channelrhodopsin Chimera C1C2 with OM3/MRCI. *ChemPhotoChem* **2019,** *3* (2), 107-116.

100.   Rajput, J.; Rahbek, D. B.; Andersen, L. H.; Hirshfeld, A.; Sheves, M.; Altoe, P.; Orlandi, G.; Garavelli, M., Probing and modeling the absorption of retinal protein chromophores in vacuo. *Angewandte Chemie* **2010,** *49* (10), 1790-3.

101.   Watanabe, H. C.; Mori, Y.; Tada, T.; Yokoyama, S.; Yamato, T., Molecular mechanism of long-range synergetic color tuning between multiple amino acid residues in conger rhodopsin. *Biophysics* **2010,** *6*, 67-68.

102.   Tajkhorshid, E.; Baudry, J.; Schulten, K.; Suhai, S., Molecular Dynamics Study of the Nature and Origin of Retinal's Twisted Structure in Bacteriorhodopsin. *Biophysical Journal* **2000,** *78* (2), 683-693.

103.   Okada, T.; Sugihara, M.; Bondar, A. N.; Elstner, M.; Entel, P.; Buss, V., The retinal conformation and its environment in rhodopsin in light of a new 2.2 A crystal structure. *J Mol Biol* **2004,** *342* (2), 571-83.

104.   Ernst, O. P.; Lodowski, D. T.; Elstner, M.; Hegemann, P.; Brown, L. S.; Kandori, H., Microbial and animal rhodopsins: structures, functions, and molecular mechanisms. *Chem Rev* **2014,** *114* (1), 126-63.

105.   Gieseking, R. L.; Risko, C.; Bredas, J. L., Distinguishing the Effects of Bond-Length Alternation versus Bond-Order Alternation on the Nonlinear Optical Properties of pi-Conjugated Chromophores. *The journal of physical chemistry letters* **2015,** *6* (12), 2158-62.

106.   Ho Choi, C.; Kertesz, M.; Karpfen, A., The effects of electron correlation on the degree of bond alternation and electronic structure of oligomers of polyacetylene. *The Journal of Chemical Physics* **1997,** *107* (17), 6712-6721.

107.   Jacquemin, D.; Adamo, C., Bond Length Alternation of Conjugated Oligomers: Wave Function and DFT Benchmarks. *J Chem Theory Comput* **2011,** *7* (2), 369-76.

108.   Mayer, I., Charge, bond order and valence in the AB initio SCF theory. *Chemical Physics Letters* **1983,** *97* (3), 270-274.

109.   Wanko, M.; Hoffmann, M.; Strodel, P.; Koslowski, A.; Thiel, W.; Neese, F.; Frauenheim, T.; Elstner, M., Calculating absorption shifts for retinal proteins: computational challenges. *The journal of physical chemistry. B* **2005,** *109* (8), 3606-15.

110.   Mao, J.; Do, N. N.; Scholz, F.; Reggie, L.; Mehler, M.; Lakatos, A.; Ong, Y. S.; Ullrich, S. J.; Brown, L. J.; Brown, R. C.; Becker-Baldus, J.; Wachtveitl, J.; Glaubitz, C., Structural basis of the green-blue color switching in proteorhodopsin as determined by NMR spectroscopy. *J Am Chem Soc* **2014,** *136* (50), 17578-90.

111.   Sekharan, S.; Katayama, K.; Kandori, H.; Morokuma, K., Color vision: "OH-site" rule for seeing red and green. *J Am Chem Soc* **2012,** *134* (25), 10706-12.

112.   Welke, K.; Frahmcke, J. S.; Watanabe, H. C.; Hegemann, P.; Elstner, M., Color tuning in binding pocket models of the chlamydomonas-type channelrhodopsins. *The journal of physical chemistry. B* **2011,** *115* (50), 15119-28.

113.   Liang, R.; Liu, F.; Martinez, T. J., Nonadiabatic Photodynamics of Retinal Protonated Schiff Base in Channelrhodopsin 2. *The journal of physical chemistry letters* **2019,** *10* (11), 2862-2868.

114.   Volkov, O.; Kovalev, K.; Polovinkin, V.; Borshchevskiy, V.; Bamann, C.; Astashkin, R.; Marin, E.; Popov, A.; Balandin, T.; Willbold, D.; Buldt, G.; Bamberg, E.; Gordeliy, V., Structural insights into ion conduction by channelrhodopsin 2. *Science* **2017,** *358* (6366).